The Astrophysical Journal, 714:549–560, 2010 May 1 doi:10.1088/0004-637X/714/1/549

TAMING THE INVISIBLE MONSTER: SYSTEM PARAMETER CONSTRAINTS FOR ϵ AURIGAE FROM THE FAR-ULTRAVIOLET TO THE MID-INFRARED

D. W. Hoard[1], S. B. Howell[2], and R. E. Stencel[3]

[1] Spitzer Science Center, California Institute of Technology, Pasadena, CA 91125, USA

[2] National Optical Astronomy Observatory, Tucson, AZ 85719, USA

[3] Department of Physics and Astronomy, University of Denver, Denver, CO 80208, USA

Received 2009 December 4; accepted 2010 March 18; published 2010 April 12

ABSTRACT

We have assembled new *Spitzer Space Telescope* IRAC observations of the mysterious binary star ϵ Aurigae, along with archival far-ultraviolet to mid-infrared data, to form an unprecedented spectral energy distribution (SED) spanning 3 orders of magnitude in wavelength from 0.1 μm to 100 μm. The observed SED can be reproduced using a three-component model consisting of a $2.2^{+0.9}_{-0.8}$ $M_{\odot}$ F-type post-asymptotic giant branch star, and a 5.9 $\pm$ 0.8 $M_{\odot}$ B5$\pm$1 type main-sequence star that is surrounded by a geometrically thick, but partially transparent, disk of gas and dust. At the nominal *HIPPARCOS* parallax distance of 625 pc, the model normalization yields a radius of 135 $\pm$ 5 $R_{\odot}$ for the F star, consistent with published interferometric observations. The dusty disk is constrained to be viewed at an inclination of $i \gtrsim 87°$, and has an effective temperature of 550 $\pm$ 50 K with an outer radius of 3.8 AU and a thickness of 0.95 AU. The dust content of the disk must be largely confined to grains larger than $\sim$10 μm in order to produce the observed gray optical–infrared eclipses and the lack of broad dust emission features in the archival *Spitzer* mid-infrared spectra. The total mass of the disk, even considering a potential gaseous contribution in addition to the dust that produces the observed infrared excess, is $\ll$1 $M_{\odot}$. We discuss evolutionary scenarios for this system that could lead to the current status of the stellar components and suggest possibilities for its future evolution, as well as potential observational tests of our model.

Key words: binaries: eclipsing – circumstellar matter – stars: AGB and post-AGB – stars: individual (Epsilon Aurigae)

Online-only material: color figures

1. INTRODUCTION

The bright star ϵ Aurigae (HD 31964) is a single-lined spectroscopic binary that is famous for its long orbital period (27.1 yr), which is punctuated by an almost two-year long eclipse caused by an essentially invisible object (Carroll et al. 1991). The central problem posed by this system is that if the F star component, which dominates the light from the system over a wide range of wavelength and is the eclipsed object, is a massive supergiant (as its spectrum implies), then the invisible companion is surprisingly underluminous for its mass. Exotic solutions for this mass conundrum involving, for example, a black hole (Cameron 1971) are not viable because of the train of ever more complicated additional requirements that observational constraints impose on such a model. For example, the lack of significant X-ray emission from the system precludes a black hole *unless* there is no accretion from the disk, which is not possible *unless* there is yet another unseen body (a massive planet, perhaps) that clears out the space around the black hole, and so on (see the discussions in Barsony et al. 1986; Carroll et al. 1991; Wolk et al. 2010).

By examining the optical spectra of ϵ Aur near the end of its 1954–1956 eclipse, Hack (1959) was able to deduce the electron density and develop the hypothesis of a Be-star-like hot object at the center of a large disk of occulting material (Hack 1961). Woolf (1973) reported pioneering infrared (IR) observations that revealed the presence of an excess consistent with the disk being a cloud of partially ionized gas, with a total projected area comparable to that of the F star. An estimate of electron density from the IR excess was consistent with the optical–ultraviolet (UV) estimates of 10^{11} cm^{-3}.

As IR detector technology advanced, Backman et al. (1984) reported ground-based IR photometry obtained during the 1982–1984 eclipse that demonstrated that the excess could be characterized as a $T = 500 \pm 150$ K source subtending 8×10^{-16} sr. Backman & Gillett (1985) refined this result with *IRAS* satellite photometry during the eclipse, extending the wavelength coverage well into the thermal IR, and yielding a revised temperature of 475 $\pm$ 50 K and angular extent of $8.6 \pm 1.0 \times 10^{-16}$ sr. Stickland (1985) examined the same *IRAS* data and was led to conclude that the disk temperature could be better characterized as a 750$\pm$100 K source with a projected area about six times that of the F star photosphere. Regardless of its exact characteristics, the transiting disk in the ϵ Aur binary offers a valuable opportunity for studying its longitudinal structure in ways not possible with circumstellar disks around single stars.

Here we report on the results from new mid-IR observations of ϵ Aur made with the *Spitzer Space Telescope* (Werner et al. 2004), which provide a more precise characterization of the occulting body, as well as a new look at archival data at shorter wavelengths, which better constrain the stellar components. The importance of this exercise lies in the fact that now the spectral energy distribution (SED) can be defined much more precisely, thanks to the availability of new and recalibrated data spanning the far-UV to the mid-IR. These results strongly imply that the putative F supergiant star in ϵ Aur is more likely a lower mass, unstable post-AGB object that previously transferred matter to a B(e)-like star companion—as proposed by Webbink (1985)—resulting in a complex "dark matter" disk (Howell et al. 2008) that causes the eclipses.

2. SED—THE DATA

To construct our SED for ϵ Aur, which spans 3 orders of magnitude in wavelength, we combined data from new

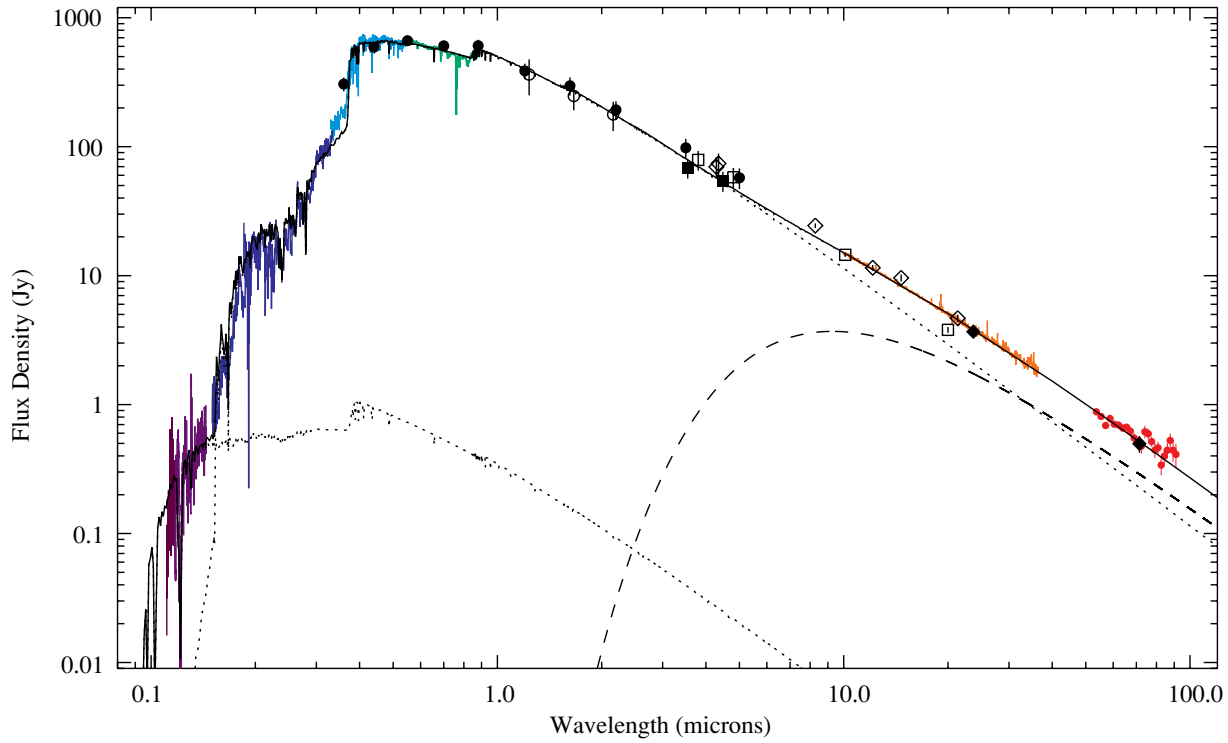

Figure 1. Observed (dereddened) SED of ϵ Aur with a three component model. From short to long wavelengths, the photometric points are U, B, V, R, I from the AAVSO (filled circles), J, H, K, L, M (filled circles), J, H, Ks from 2MASS (unfilled circles), IRAC from *Spitzer* (filled squares), ground-based L', M, N, Q (unfilled squares), $B1$, $B2$, A, C, D, E bands from *MSX* (unfilled diamonds), and MIPS from *Spitzer* (filled diamonds). Vertical error bars are the photometric uncertainties (which are dominated by the systematic uncertainty of the dereddening process for the dereddened data). The spectroscopic data are *FUSE* (dark purple), *HST*-GHRS (light purple), *IUE* (dark blue), ground-based optical (light blue and green), IRS (orange), and MIPS-SED (filled red squares) from *Spitzer*. See the text and Table 1 for more information about the data. The model (solid line) is the sum of limb-darkened model F0 (post-AGB) and B5 V spectra (dotted lines), and a cool blackbody disk (dashed line). See the text and Table 2 for more information about the model.

observations in the mid-IR from *Spitzer*, recent observations from the American Association of Variable Star Observers (AAVSO) in the optical, and archival ground- and space-based observations at other wavelengths. The space-based data in particular come from the *Midcourse Space Experiment* (*MSX*), the *International Ultraviolet Explorer* (*IUE*), the *Hubble Space Telescope* (*HST*), and the *Far-Ultraviolet Spectroscopic Explorer* (*FUSE*). The SED data are listed in Table 1 and plotted in Figure 1. All of the observations were obtained outside of eclipse phases; the majority was obtained prior to the onset of the eclipse that began in late 2009, but well after the end of the prior eclipse in 1984, except as noted in Table 1. We describe our new *Spitzer* mid-IR observations in more detail below.

2.1. Spitzer *IRAC*

The expected flux density of ϵ Aur at 3–5 μm exceeds the nominal saturation limits of channels 1 (3.6 μm) and 2 (4.5 μm) of the IRAC (Fazio et al. 2004) on *Spitzer* by factors of several times. The rationale for observing ϵ Aur with IRAC was two-fold: (1) as a test case for a potential monitoring campaign whose cadence could not be accomplished from the ground and (2) to obtain measurements in the 3–5 μm range whose flux calibration is homogenous with that of the other *Spitzer* data already obtained at longer wavelengths (see Sections 2.2 and 2.3). As it turned out, a third reason became apparent after the fact; namely, that existing older IR data in this wavelength range are not directly comparable to the more recent longer wavelength *Spitzer* data (see discussion in Section 3.4).

We utilized an allocation of six minutes[4] of Director's Discretionary Time in late April 2009, shortly before depletion of the *Spitzer* cryogen in mid-May 2009. We used a novel observing strategy that took advantage of both the extremely short exposure time available in the IRAC sub-array mode and the specific placement of the target centroid at the intersection of 4 pixels. The latter condition spreads the total illumination of the detector, as well as the brightest part of the point response function (PRF), over the maximum number of pixels. In sub-array mode, observations are obtained in units of 64 exposures of a 32 × 32 pixel section of the full 256 × 256 pixel array, and are tiled onto the full array for downlink. This resulted in four dithered observations of ϵ Aur in each channel, with each dither comprised of 64 consecutive 0.02 s exposures.

We initially applied the IRAC array-location-dependence correction to the individual sub-array images, as described in the IRAC Data Handbook,[5] and then performed aperture photometry on them (e.g., as described in Hoard et al. 2009) using the IRAF[6] task PHOT. We utilized a 10 pixel radius aperture (1 pixel ≈ 1.″22), with a 10–20 pixel background annulus, which is the configurations for which the corresponding aperture corrections are 1.00 in all IRAC channels.

The high time resolution and photon-abundant nature of these observations revealed two interesting instrumental artifacts that are normally below the detection threshold in *Spitzer*

[4] Three minutes of which were the standard "slew tax" applied to all *Spitzer* observations.
[5] See http://ssc.spitzer.caltech.edu/irac/dh/.
[6] IRAC is maintained and distributed by the National Optical Astronomy Observatory.

Table 1
The Data

Wavelength (μm)	Band	Source	Date of Observation: UT (YYMMDD)	Date of Observation: JD (JD-2400000)	Orbital Phase[a]	Flux Density: Observed[c] (Jy)	Flux Density: Dereddened[d] (Jy)	Reference[d]	Notes
0.111–0.117	Spectrum	*FUSE*	010107	51917	0.646	0.00025–0.0015	0.15–0.3	Ake (2006)	···
0.117–0.146	Spectrum	*HST*-GHRS	960216	50130	0.466	0.002–0.02	0.4–1.2	Sheffer & Lambert (1999)	···
0.150–0.198	Spectrum	*IUE*-SWP	850203, 850317	46099, 46141	0.058–0.062	0.005–0.8	0.6–20	Sheffer & Lambert (1999)	(1, 2)
0.185–0.335	Spectrum	*IUE*-LWP	861119–861123	46753–46757	0.124–0.125	0.5–48	10–130	Sheffer & Lambert (1999)	(2, 3)
0.329–0.549	Spectrum	ground	820405	45065	0.953	25–215	150–630	Thompson et al. (1987)	(4)
0.567–0.889	Spectrum	ground	c.1990–1992	c.47892–48987	0.25–0.33	240–330	660–520	Torres-Dodgen & Weaver (1993)	(5)
0.360	*U*	AAVSO	031101–090701	52918–55013	0.748–0.959	59.1 ± 1.8	306.0 ± 37.6	This work	(6)
0.44	*B*	AAVSO	031101–090701	52918–55013	0.748–0.959	148.4 ± 4.5	591.5 ± 49.4	This work	(6)
0.55	*V*	AAVSO	031101–090701	52918–55013	0.748–0.959	230.4 ± 6.9	663.9 ± 59.3	This work	(6)
0.70	*R*	AAVSO	031101–090701	52918–55013	0.748–0.959	294.6 ± 8.8	605.8 ± 55.9	This work	(6)
0.88	*I*	AAVSO	031101–090701	52918–55013	0.748–0.959	378.4 ± 11.4	606.8 ± 67.9	This work	(6)
1.20	*J*	ground	970907–000418	50699–51652	0.523–0.620	297.1 ± 10.3	386.9 ± 53.4	Taranova & Shenavrin (2001)	(7)
1.235	*J*	2MASS	991108	51491	0.603	282.2 ± 78.6	362.5 ± 112.3	Skrutskie et al. (2006)	···
1.62	*H*	ground	970907–000418	50699–51652	0.523–0.620	254.8 ± 14.0	296.8 ± 47.5	Taranova & Shenavrin (2001)	(7)
1.662	*H*	2MASS	991108	51491	0.603	213.6 ± 35.5	247.1 ± 55.5	Skrutskie et al. (2006)	···
2.159	*Ks*	2MASS	991108	51491	0.603	162.5 ± 32.4	177.7 ± 45.4	Skrutskie et al. (2006)	···
2.20	*K*	ground	970907–000418	50699–51652	0.523–0.620	177.1 ± 6.1	193.1 ± 31.7	Taranova & Shenavrin (2001)	(7)
3.50	*L*	ground	970907–000418	50699–51652	0.523–0.620	94.5 ± 3.3	98.0 ± 16.9	Taranova & Shenavrin (2001)	(7)
3.544	IRAC-1	*Spitzer*	090426	54948	0.953	66.2 ± 3.0	68.6 ± 12.0	This work	(8)
3.8	L'	ground	811113	44922	0.939	76.5 ± 2.6	79.0 ± 13.7	Backman et al. (1984)	(4, 9)
4.29	*MSX*-B1	*MSX*	c.960424–970222	c.50198–50502	0.47–0.50	67.9 ± 6.1	69.7 ± 13.4	Egan et al. (2003)	···
4.35	*MSX*-B2	*MSX*	c.960424–970222	c.50198–50502	0.47–0.50	72.1 ± 6.6	74.0 ± 14.3	Egan et al. (2003)	···
4.479	IRAC-2	*Spitzer*	090426	54948	0.953	52.9 ± 2.4	54.2 ± 9.6	This work	(7)
4.8	*M*	ground	800130–811210	44269–44949	0.873–0.942	56.8 ± 2.9	58.0 ± 10.4	Backman et al. (1984)	(4, 9)
5.00	*M*	ground	970907–000418	50699–51652	0.523–0.620	56.3 ± 3.4	57.4 ± 10.5	Taranova & Shenavrin (2001)	(7)
8.28	*MSX*-A	*MSX*	c.960424–970222	c.50198–50502	0.47–0.50	24.4 ± 1.0	···	Egan et al. (2003)	···
9.89–37.14	IRS-1, -3	*Spitzer*	051019, 060317	53663, 53812	0.823, 0.838	15.3–5.1	···	This work	(1, 10)
10.1	*N*	ground	800201–811217	44271–44956	0.873–0.942	14.5 ± 0.5	···	Backman et al. (1984)	(4, 9)
12.13	*MSX*-C	*MSX*	c.960424–970222	c.50198–50502	0.47–0.50	11.5 ± 0.6	···	Egan et al. (2003)	···
14.65	*MSX*-D	*MSX*	c.960424–970222	c.50198–50502	0.47–0.50	9.6 ± 0.6	···	Egan et al. (2003)	···
20.0	*Q*	ground	811210–811217	44949–44956	0.942	3.8 ± 0.2	···	Backman et al. (1984)	(4, 9)
21.34	*MSX*-E	*MSX*	c.960424–970222	c.50198–50502	0.47–0.50	4.7 ± 0.3	···	Egan et al. (2003)	···
23.675	MIPS-24	*Spitzer*	050925, 060223	53639, 53790	0.820, 0.836	3.7 ± 0.2	···	This work	(1, 11)
53.7–91.1	MIPS-SED	*Spitzer*	050925, 060223	53639, 53790	0.820, 0.836	0.88–0.41	···	This work	(1, 12, 13)
71.44	MIPS-70	*Spitzer*	050925, 060223	53639, 53790	0.820, 0.836	0.5 ± 0.07	···	This work	(1, 11)

Notes. (1) Flux densities are the averages of two measurements on the indicated dates. (2) *IUE* exposures SWP 25156 and 25470, and LWP 09565, 09547, and 09554. (3) Flux densities are the averages of three measurements in the indicated date range. (4) Note that the orbital phase refers to the previous cycle (i.e., before the 1982–1984 eclipse). (5) Exact date of spectrum is not given in the corresponding publication. (6) Flux densities are the averages of N data points in the indicated date range: $N_{\rm U} = 411$, $N_{\rm B} = 411$, $N_{\rm V} = 411$, $N_{\rm R} = 37$, $N_{\rm I} = 21$. (7) Flux densities are the averages of 34 measurements in the indicated date range. (8) *Spitzer* AOR key 33903360, processing pipeline version S18.7.0. (9) Flux densities are the averages of N pre-eclipse data points in the indicated date range: $N_{\rm L'} = 1$, $N_{\rm M} = 4$, $N_{\rm N} = 4$, $N_{\rm Q} = 2$. (10) *Spitzer* AOR keys 13848832 and 13849600, processing pipeline version S18.7.0. (11) *Spitzer* AOR keys 13849088 and 13850112, processing pipeline version S16.1.0. (12) *Spitzer* AOR keys 13849856 and 13849344, processing pipeline version S16.1.0. (13) MIPS-SED flux densities have been normalized to the MIPS-70 photometric point by scaling the former by a factor of 0.84.

[a] Using the orbital ephemeris $\rm JD_{obs} = JD2445525+9890E$ (e.g., Schmidtke et al. 1985; Carroll et al. 1991).

[b] See the text for a discussion of the dereddening applied to the data.

[c] When necessary, photometric data reported in magnitudes were converted to flux densities using appropriate filter-specific zero-point values (e.g., see Cohen et al. 2003; Bessell & Brett 1988; Campins et al. 1985; Bessell 1979; Beckwith et al. 1976; Mendoza V. 1963).

[d] For this work, we have re-extracted all photometric and spectroscopic measurements from archival data, but list here the first original publication of the relevant data.

IRAC observations: a rapid "jitter" with amplitude of ≈1% in the measured flux densities in each sequence of sixty-four 0.02 s exposures, as well as overall trends with slopes of 1%–2% in measured flux density during each 64 frame sequence. The former effect is caused by sub-pixel mismatch between the measured and actual centroid of the PRF, propagated through the normal IRAC pixel-phase correction, which accounts for the exact position of the target centroid *within* a pixel. It is likely caused by resolving the small discrete steps in the *Spitzer* tracking motion.

The latter effect appears to be linked to the telescope settle time of 2 s after a slew or dither offset, which is longer than the ≈1.5 s total length of one of the 64 frame sub-array sequences. Both of these effects are presumably present during the first 2 s of any normal, full-array IRAC exposure, for which the shortest available exposure time is 2 s. Consequently, in a full-array observation of a fainter target, these effects are not time-resolved and are below the level of photon counting noise, so go unnoticed in the final, single photometric measurement per observation. In addition, we see the offsets of order several percent between mean flux densities at different dither positions (caused by pixel-to-pixel variations) that are also found in dithered full-array observations, and are mitigated by averaging together the flux densities measured at the different dither positions.

Additionally, in the channel 2 observations, we see a steep linear trend in the measured flux densities in each of the four dithered sequences of 64 exposures. This results in an increase of ≈5%–7%, with approximately equal slope from the start to the end of each dither sequence. This could possibly include a contribution from the so-called "ramp" effect noticed in some exoplanet transit light curves obtained with IRAC (Deming 2009), but, considering the very short total duration of these exposure sequences, is more likely due to build-up of latents on the pixels exposed to ϵ Aur during each sub-array sequence. This particular artifact is *not* present in our channel 1 data. We note that a 2.5 hr sequence of deep IRAC exposures in the Oph star-forming region ended about an hour before our ϵ Aur observation, and immediately prior to our observations there was a short (20 minutes) series of observations in the Galactic plane. So, it is entirely possible that the charge traps in channel 1 that would lead to latents were already full when our observation started.

The final photometric measurements reported in Table 1 were obtained as follows: for channel 1 (IRAC-1), in order to mitigate against one saturated pixel in the ϵ Aur PRF during the first dither sequence, we combined all 256 sub-array images using the *Spitzer* data analysis software tool MOsaicker and Point source EXtractor (MOPEX),[7] and performed aperture photometry (as described above) on the mosaic. This results in a flux density that is 0.3 Jy fainter than the value obtained by averaging together the aperture photometry results for all 256 individual sub-array exposures, including the one saturated pixel in 64 exposures. Qualitatively, this result is consistent with the removal of the saturated pixel in 64 of the images, resulting in a slightly smaller "true" flux density measurement. For channel 2 (IRAC-2), there are no saturated pixels in any of the individual sub-array images; however, in order to mitigate against the latent charge effect described above, we averaged together only the first five exposures in each dither sequence. In addition, we had to utilize a 5 pixel aperture (with 5–10 pixel background annulus) because the 10 pixel aperture was partially off the sub-array during two of the dither sequences. This required use of the corresponding aperture correction for IRAC-2 of 1.064.

In all cases, as described in the IRAC Data Handbook, we applied the pixel-phase correction (Hora et al. 2008) to the photometry in both channels. However, we did not perform the color correction other than to utilize the isophotal effective channel wavelengths (see Table 1) during our subsequent interpretation of the data, which accounts for almost all of the color correction. The remaining effect of the color correction is folded into our IRAC systematic uncertainty budget. As described, in more detail, in Hoard et al. (2009), the total uncertainty budget for IRAC photometry includes several systematic terms (3% for the absolute gain calibration, 1% for repeatability, 3% for the absolute flux calibration of the IRAC calibration stars, and 1% for the color correction), as well as a scatter term evaluated from the rms scatter of the individual flux density measurements after removing all long timescale trends. The uncertainties in the IRAC photometry values listed in Table 1 reflect these terms added in quadrature.

2.2. *Spitzer* Infrared Spectrograph

A *Spitzer* GO-2 observing program (20058; Stencel 2007) on ϵ Aur obtained observations with the Infrared Spectrograph (IRS; Houck et al. 2004) and MIPS (see below). For this work, we have utilized the current mature pipeline-(re)processed data for those observations, and re-extracted final data products. The two high resolution IRS modules were used during two visits to ϵ Aur, and we utilized the *Spitzer* data analysis software tool *Spitzer* IRS Custom Extraction (SPICE)[8] to extract the calibrated spectra from each visit for each of the two nod positions from the combined post-BCD data products (which simply co-add the three individual cycle exposures at each nod position from each visit). Module 1 spans 9.9–19.5 μm, while module 3 spans 18.8–37.1 μm, at a resolving power of ∼600 in both modules. Prior to extraction, the *Spitzer* data analysis software tool IRSCLEAN[9] was used to remove both permanent and rogue hot pixels from the combined post-BCD images. Because of the short exposure times used for individual frames (6 and 14 s in modules 1 and 3, respectively), as well as the brightness of the target, no offset sky background spectrum was subtracted; this is in keeping with the "best practices" recommendation for observations of this type from the *Spitzer* Observer's Manual.[10] The four extracted spectra from each module (two nods from each of two visits) were then combined in a weighted average after rejecting all wavelength points flagged as unreliable by SPICE.

2.3. MIPS

The MIPS (Rieke et al. 2004) data on ϵ Aur were obtained in two observing modes. The first of these was the normal small field photometry mode at 24 and 70 μm (MIPS-24 and MIPS-70, respectively). We performed aperture photometry on the filtered combined post-BCD images following the procedures in the MIPS Data Handbook[11]; operationally, this process is very similar to that used to obtain the IRAC photometry. For the MIPS-24 images, we utilized a 35 arcsec aperture with a

[7] See http://ssc.spitzer.caltech.edu/postbcd/mopex.html

[8] See http://ssc.spitzer.caltech.edu/postbcd/spice.html.

[9] See http://ssc.spitzer.caltech.edu/postbcd/irsclean.html.

[10] See http://ssc.spitzer.caltech.edu/warmmission/propkit/som/.

[11] See http://ssc.spitzer.caltech.edu/mips/dh/index.html.

Table 2
The Model

Component	Parameter	Value	Reference
System	Adopted Distance, d (pc)	625	*HIPPARCOS* (Perryman et al. 1997)
	Inclination, i (°)	89 ($\gtrsim$87)	This work, Lissauer et al. (1996)
	Orbital Separation, a (AU)	$18.1^{+1.2}_{-1.3}$	This work
F Star	Spectral Type	F0 II–III? (post-AGB)	This work
	Temperature, $T_{\rm F}$ (K)	7750	This work, Castelli (1978)
	log g	$\lesssim$1.0	This work, Castelli (1978)
	Radius, $R_{\rm F}$ ($R_\odot$)	135 $\pm$ 5	This work
	Angular Diameter, D_α (mas)	2.01 $\pm$ 0.07	This work
	Mass, $M_{\rm F}$ ($M_\odot$)	$2.2^{+0.9}_{-0.8}$	This work
B Star	Spectral Type	$B5 \pm 1\ V$	This work
	Temperature, $T_{\rm B}$ (K)	15,000	Cox (2000)
	log g	4.0	Cox (2000)
	Radius, $R_{\rm B}$ ($R_\odot$)	3.9 $\pm$ 0.4	Cox (2000)
	Mass, $M_{\rm B}$ ($M_\odot$)	5.9 $\pm$ 0.8	Cox (2000)
Disk	Temperature, $T_{\rm disk}$ (K)	550 $\pm$ 50	This work
	Radius, $R_{\rm disk}$ (AU)	$3.8^{+0.1}_{-0.4}$	This work, Lissauer et al. (1996)
	Height, $H_{\rm disk}$ (AU)	0.475	This work
	Assumed Mass, $M_{\rm disk}$ ($M_\odot$)	$\ll$1	This work
	Inferred Dust Grain Radius, $r_{\rm grain}$ (μm)	$\gtrsim$10	This work, Lissauer et al. (1996)
	Transmissivity Factor	0.3	This work
	Emissivity Factor	2.43	This work

40–50 arcsec background annulus, and applied the corresponding aperture correction of 1.08. For the MIPS-70 images, we utilized a 35 arcsec aperture with a 39–65 arcsec background annulus, and applied the corresponding aperture correction of 1.22. As with the IRAC photometry, we did not apply the color correction because most of it is accounted for by utilizing the isophotal band wavelengths (see Table 1). Instead, we folded the remaining small effect into our uncertainty budget.

For MIPS-24 photometry, the total systematic uncertainty budget is the quadrature sum of 4% for the absolute calibration, 0.4% for repeatability, 3% for the color correction, and 5% for the aperture correction. These values reflect upper limits from version 3.3 of the MIPS Data Handbook. In addition, the total uncertainty includes a scatter term of 0.006 Jy (0.2%) obtained for the target aperture in the uncertainty ("munc") image provided as part of the post-BCD data products. For the MIPS-70 photometry, the corresponding terms in the uncertainty budget are 7% for the absolute calibration, 5% for repeatability, 3% for the color correction, 5% for the aperture correction, and a scatter term of 0.007 Jy (1.4%).

The other MIPS observation utilized the MIPS-SED mode, which obtains a very low resolution ($R \approx$ 15–25) spectrum between 52 and 97 μm. We performed a weighted average of the post-BCD extracted spectrum from each of the two MIPS-SED visits to ϵ Aur. The flux calibration uncertainty for MIPS-SED mode is ~20%, and we found it necessary to scale the data by a factor of 0.84 (i.e., a 16% reduction compared to the extracted values) in order to match the MIPS-SED spectrum with the better calibrated MIPS-70 photometric point.

3. SED—THE MODEL

It has been fairly well established (e.g., see Huang 1965, Kopal 1971, and the review in Webbink 1985) that the ϵ Aur system consists of three primary components: an F star orbited by one or two B stars, with a large dusty disk surrounding the latter. It is the disk that eclipses the F star every 27 years. The exact details of these components, however, remain rather nebulous; for example, the mass of the F star has been proposed to be either very high (10–20 $M_\odot$; e.g., Lissauer et al. 1996) or relatively low (1–4 $M_\odot$; e.g., Lissauer et al. 1996; Saito et al. 1987; Takeuti 1986). The disk around the B star has been variously described as thick or thin, flat or twisted, edge-on or slightly inclined, opaque or semi-transparent, and "solid" or containing a central void.

Fortunately, in the nearly three decades since its last eclipse, some important new information about ϵ Aur has been obtained. This includes a *HIPPARCOS* trigonometric parallax distance (with a nominal value of 625 pc, which we have used in our model calculations below; Perryman et al. 1997), various interferometric measurements of the angular size of the F star (≈2.1–2.3 mas from 0.45 μm to K band; Stencel et al. 2008; Mozurkewich et al. 2003; Nordgren et al. 2001), and the space-based far-UV and mid-IR observations shown in Figure 1, which reveal details about the system components that are *not* the F star (which otherwise completely dominates the SED of ϵ Aur in the range 0.2–4 μm). Using these data, we are now able to definitively constrain some of these heretofore uncertain system parameters. Our observed and model SEDs are shown in Figure 1 and the model parameters are listed in Table 2. We discuss the model parameters, constraints, and components in more detail below.

3.1. Dereddening of the Observed SED

The observed flux densities were dereddened using the UV–optical–IR extinction law from Fitzpatrick & Massa (2007). For $\lambda > 5\,\mu$m, the reddening correction was negligible, so was not applied to the data. An interstellar reddening to ϵ Aur, $E(B-V) = +0.38$, was used for $\lambda = 0.33$–$5\,\mu$m. This value was fine-tuned from a starting value of $E(B-V) = +0.35$ in the range $E(B-V) \approx 0.3$–0.4 found in the literature (e.g., Mozurkewich et al. 2003; Torres-Dodgen & Weaver 1993; Stickland 1985; Ake 1985; Hack & Selvelli 1979; Castelli 1978; Hobbs 1969), in order to best match the optical spectra and photometry in the SED to the model F star spectrum. We note that the apparent disagreement between the optical spectrum

at the shortest wavelengths, near 0.3 μm, most likely reflects issues in accurately calibrating a ground-based UV spectrum, rather than an actual disagreement with the model, since the model matches the flux density of the *IUE* spectrum that ends at 0.3 μm quite well. At wavelengths shortward of $\lambda = 0.33\,\mu$m, additional dereddening was applied—see Section 3.3 for details.

3.2. The F Star

We utilized the $T = 7750$ K, $\log g = 1.0$ (Castelli 1978), solar abundance model spectrum from the grid of Castelli & Kurucz (2003)[12] to represent the F star component in ϵ Aur, which has the *appearance* (more on that later) of an F0 supergiant star.

We applied limb-darkening to the model spectrum using the Van Hamme (1993) relation, which is linear in form with wavelength-, temperature-, and gravity-dependent coefficients. The optical–near-IR region of the SED is dominated by this component, and we scaled the limb-darkened model spectrum to match the *J*-band photometric point from Taranova & Shenavrin (2001; Table 1). This requires a radius of $R_{\rm F} = 135\,R_\odot$, resulting in an angular diameter of 2.01 mas. The radius can only be changed by $\pm 5\,R_\odot$, corresponding to ± 0.07 mas in angular diameter, without significantly worsening the match to the J point. Our model angular diameter is somewhat smaller than the value of 2.27 ± 0.11 mas measured by Stencel et al. (2008) in the *K* band, but is in agreement within 2σ.

The expected surface gravity of a "normal" F0 supergiant with radius of 135 $R_\odot$ and mass of 15–20 $M_\odot$ is $\log g \approx 1.5$, which is one-half dex larger than the value selected for our model spectrum for this component. However, as we will demonstrate below, the mass of the F star in ϵ Aur is significantly lower than that of a normal F supergiant. In fact, a more appropriate value for the gravity would be $\log g = 0.5$; unfortunately, model spectrum calculations apparently are not typically made for stars that look like F supergiants but have masses an order of magnitude smaller, so $\log g = 1.0$ is the lowest gravity model available. In any case, the gross differences in the model spectra between $\log g$ values of 1.0, 1.5, and 2.0 can be compensated for by changing the stellar radius by only a few percent, comparable to the determined $\pm 5\,R_\odot$ uncertainty, so we expect no significant difference in the overall appearance of the model SED.

3.3. The B Star

Shortward of $\approx$0.15 μm, the F star spectrum drops off sharply, and the B star spectrum dominates the SED of ϵ Aur. This far-UV wavelength region (see Figure 2) provides the primary constraint on the spectral type (and, hence, mass and radius) of the B star. Using the interstellar dereddening of the observed SED (see Section 3.1), a B8 V star (represented by the limb-darkened, $T = 12{,}000$ K, $\log g = 4.0$, solar abundance model spectrum from Castelli & Kurucz 2003) initially provides a good match to the observed SED in this region, with the exception that the Lyα absorption line in the model spectrum is significantly broader and deeper than observed in the *HST* Goddard High Resolution Spectrograph (GHRS) spectrum of ϵ Aur.

However, the B star is completely embedded in the dusty disk, which is viewed close to edge-on and has a significantly larger thickness than the radius of any B-type main-sequence star (see Section 3.4). Consequently, we must consider that the observed spectral contribution of the B star will necessarily have been modified by passage through the disk. There are two likely effects. The first is that the observed spectral contribution of the B star will be overall fainter compared to the unobscured case; this is essentially the same thing that happens to the F star during eclipse, but affects the B star at all times. In the example mentioned above, the B8 V star is only a good match to the observed SED if the disk is completely transparent, which, among other inconsistencies, would preclude the possibility of the disk eclipsing the F star.

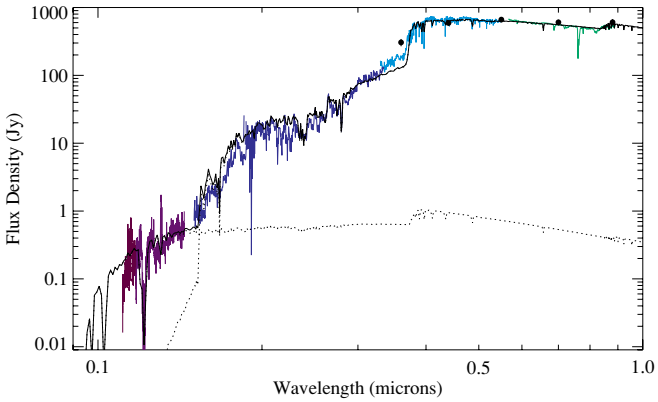

Figure 2. Expanded view of the ultraviolet wavelength region of Figure 1.
(A color version of this figure is available in the online journal.)

At optical–near-IR wavelengths, the eclipse of ϵ Aur has been observed to be approximately gray (e.g., Kopal 1971; Lissauer et al. 1996). This is taken as evidence that the dust grains in the disk around the B star must be relatively large, a conclusion that is also supported by the lack of broad dust emission features in the *Spitzer* IRS spectrum of ϵ Aur (see Figure 3), which implies dust grains of size $\gtrsim$10 μm (see Morales et al. 2009; Natta et al. 2007; D'Alessio et al. 2006; and references therein, for discussions of the effect of dust grain size on observed spectral features). We can simulate this effect by applying a simple scaling factor (which we will refer to as the disk "transmissivity" factor) to the B star model spectrum. A transmissivity factor of 1.0 would correspond to a completely transparent disk, such that the light from an object inside or behind the disk would be unaffected. On the other hand, a transmissivity factor of 0.0 would correspond to a completely opaque disk, such that the light from an object inside or behind the disk would be completely blocked. For example, if the disk attenuates the spectral contribution of the B star by 50% (a transmissivity factor of 0.5), then the observed SED could still be matched by the presence of two B8 V stars, corresponding to the close binary B star model suggested by Lissauer & Backman (1984) and Eggleton & Pringle (1985).

The second likely effect on the observed B star spectrum introduced by the circumstellar disk is an additional reddening. The difficulty of distinguishing between the observable effects of interstellar and circumstellar material is often noted (e.g., Hempel & Schmitt 2003; Holweger et al. 1999; Wood et al. 1997). In the case of ϵ Aur, we have the relative advantage that the interstellar reddening can be determined in the optical region of the spectrum. In this region, the F star dominates the light from the system, and is unaffected by the dusty disk (outside of eclipse). However, this still leaves the question of how to account for the circumstellar reddening of the B star.

To first order, additional circumstellar reddening of the B star might be blamed on the fact that the effect of reddening

[12] The grid of model spectra is available at http://wwwuser.oat.ts.astro.it/castelli/grids.html and ftp://ftp.stsci.edu/cdbs/grid/ck04models/.

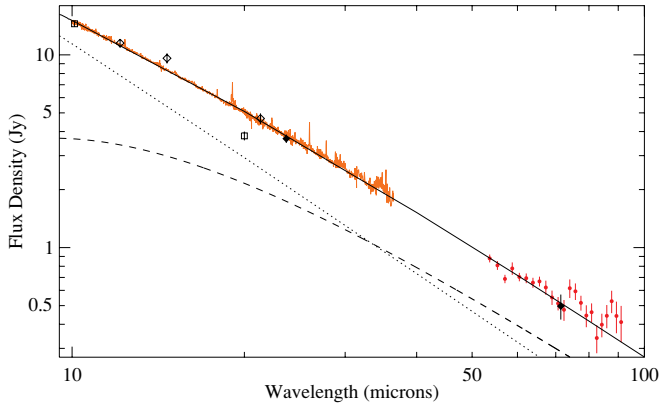

Figure 3. Expanded view of the mid-infrared wavelength region of Figure 1. (A color version of this figure is available in the online journal.)

is an order of magnitude greater in the UV than in the optical. Consequently, the "grayness" of the disk could begin to break down at the short wavelengths at which the B star spectrum dominates the SED. There is some disagreement in the literature whether this effect is (Parthasarathy & Frueh 1986; Altner et al. 1984) or is not (Ferluga & Hack 1985) supported by UV observations with *IUE*.

Another plausible scenario is that the hot B star is surrounded by a localized shell or torus of gas and small dust grains created by the sublimation and photo-spallation of the large dust grains that comprise the bulk of the disk (also see Chapman et al. 1983). This material would produce an additional non-gray attenuation of the B star's spectrum, without affecting the bulk properties of the entire disk. To account for this, we applied additional dereddening, corresponding to a larger value of $E(B-V)$, to just the B star-dominated portion of the SED. We used the Fitzpatrick & Massa (2007) reddening law, thereby making the implicit assumption that extinction caused by the localized material around the B star has the same wavelength dependence as that of the interstellar medium (ISM). We note that this scenario is consistent with the suggested presence of a "hole" (probably a decrease in optical depth rather than an actual absence of disk material) at the center of the ϵ Aur disk, which has been proposed by Wilson (1971) and others to explain the mid-eclipse brightening observed during the 1982–1984 eclipse. We do not further consider the hole since we are not concerned with the eclipse behavior, except in as much as the typical eclipse depth implies that a specific fraction of the F star's light is blocked—see Section 3.6.

The additional dereddening correction was applied to the UV region of the SED as follows. For $\lambda < 0.15\,\mu$m, the SED is completely dominated by the B star component, so we simply applied a larger dereddening (i.e., interstellar+circumstellar) to these data than to the rest of the SED data (i.e., interstellar only). We applied a combined dereddening corresponding to $E(B-V) = +0.45$ (reddening steps of +0.05 in $E(B-V)$ between $E(B-V) = +0.40$ and +0.70 were considered). For $\lambda = 0.15$–$0.33\,\mu$m, the SED is dominated by neither the B star nor the F star component. In order to construct the final dereddened data in this wavelength range (consisting of the *IUE* spectra), we first created two versions of the data dereddened using $E(B-V) = +0.38$ (interstellar only) and $E(B-V) = +0.45$ (interstellar+circumstellar), and summed them after weighting by the relative contributions of the stellar components to the total SED. For example, at $\lambda \approx 0.15\,\mu$m, the two stars contribute almost equally, whereas at $\lambda \approx 0.3\,\mu$m the B star component contributes less than 1% of the total flux density.

In the case of two B8 V stars (as discussed above), in the presence of even a small amount of additional circumstellar reddening, corresponding to $E(B-V) = 0.40$ (i.e., an increase of only 0.02 mag compared to the interstellar reddening alone), the disk transmissivity must be increased to 0.7 to preserve the match to the observed SED. For reddening corrections of $E(B-V) \geqslant 0.45$, the B8 V model continuum slope no longer matches that of the observed SED, with the latter being flatter than the former at wavelengths $< 0.15\,\mu$m. Producing the best fit for these larger circumstellar reddenings, which matches the model to the SED at $0.15\,\mu$m, and progressively underestimates the observed SED flux density at shorter wavelengths, requires a disk transmissivity of $\geqslant$0.95 for $E(B-V) \geqslant 0.45$, respectively. This is, again, ruled out by the constraint that the disk cannot be completely transparent *and* eclipse the F star.

However, a single B5V star (the next available earlier spectral type, represented by the limb-darkened, $T = 15{,}000$ K, $\log g = 4.0$, solar abundance model from Castelli & Kurucz 2003), combined with a disk transmissivity of 0.3, provides a good match to the UV region of the SED. This includes a much improved match to the width and depth of the observed Lyα absorption line (see Figure 2), which is significantly broader and deeper in the B8 V model, and increasingly too narrow and shallow for B3 V and earlier spectral type models (see below).

Spectral types of B3 V (the next available model template) or earlier for the B star are not viable solutions (even after considering additional attenuation and/or reddening by the disk) because as the B star becomes hotter, the continuum slope in this region becomes incompatible with the observed (dereddened) SED. Specifically, while the observed SED continuum slope rises toward longer wavelengths up to $0.15\,\mu$m (at which point the B star ceases to dominate the SED), the continuum of a B3 V star is almost flat and the continuum of a B0 V star has started to rise slightly toward shorter wavelengths. This holds true even after testing by the application of implausibly large additional dereddenings. Hence, the B star spectral type is fairly tightly constrained to B5 V, with an uncertainty of approximately one spectral type in either direction.

3.4. The Dusty Disk

At a wavelength of ≈3–4 μm, the observed SED of ϵ Aur begins to show a deviation from the F star spectrum. This manifests as an IR excess such that, at $100\,\mu$m, the observed SED flux density is ≈3 times brighter than that of the F star alone.[13]

We must draw a distinction between the *Spitzer* data, which were obtained at orbital phases of ≈0.8–0.95, and the other mid-IR data (from the ground and *MSX*), which were obtained at an orbital phase of ≈0.5. The latter data are systematically somewhat brighter than the IRAC data in the ≈3–5 μm region, and show some deviations at longer wavelengths, as well. Some of this behavior, particularly the stochastic deviations at the longer wavelengths, can likely be attributed to the difficulties

[13] We note that Altenhoff et al. (1994) measured a 250-GHz (1200-μm) flux density for ϵ Aur of 9 ± 2 mJy, which is more than an order of magnitude brighter than the Rayleigh–Jeans extrapolation of the F star model spectrum at that wavelength, $f_{\mathrm{F},1200} = 0.8$ mJy. In fairness, this is also a factor of 3 brighter than the sum of the flux densities of the F star and blackbody models discussed here at 1200 μm, which is 1.3 mJy. This possibly implies that there are non-thermal emission processes contributing at extremely long wavelengths.

in calibrating ground-based mid-IR photometry. However, the systematic difference at the shorter IR wavelengths suggests an actual difference in the characteristics of the cool component, either since before the 1982–1984 eclipse (when the Backman et al. 1984 data were obtained), or within an orbital cycle since after the last eclipse. The latter scenario is consistent with viewing the hotter side of the disk that is most irradiated by the F star in the data from $\phi \approx 0.5$, compared to the case in the *Spitzer* observations, when the opposite, cooler side of the disk is most visible. This effect has been noted in the past (e.g., Taranova & Shenavrin 2001; Lissauer et al. 1996), and the relevant IR data shown in Figure 1 are consistent with a suggested blackbody temperature of 800–1000 K (having peak flux density at 5–6 μm) for the hot side of the disk. Future improvements to the disk model would benefit from a well-sampled IR data set that spans the entire orbital cycle of ϵ Aur; of course, the long orbital period makes this difficult to obtain in practice.

In the meantime, we have concentrated on reproducing the IR excess delineated by the *Spitzer* data, since these data extend to the longest IR wavelengths in our data set, and have a homogenous, well-tested flux calibration. This IR excess can be reproduced remarkably well with a simple single-temperature (550 K) blackbody function, which has peak flux density at $\approx$9 μm. A χ^2 minimization test applied to the data longward of 1 μm (excluding the data longward of 3 μm that were obtained near orbital phase 0.5; see above) gives a best range of 500–600 K for the temperature. This is the range within which the change in χ^2 is less than 10% compared to the χ^2 minimum (which occurs at $T_{\rm bb} = 550$ K). Coincidentally, it is also the range within which the change in χ^2 in temperature steps of 25 K is always less than 10%.

Lissauer et al. (1996) calculated a detailed model for the disk in ϵ Aur, but for our purposes, it is not necessary to use a model that is so complex. We acknowledge that our model deals with the disk in terms of averaged bulk properties (uniform cylindrical volume with a uniform mass distribution) rather than more "realistic" characteristics such as a specific radial density profile, scale height, and so on. The difficulty of specifying the detailed physics of such a disk, in the absence of sufficient constraints, is clear from the discussions in Lissauer et al. (1996) and Carroll et al. (1991). However, it is also clear that the SED is reproduced very well by a parametrically simple model. Thus, the task of reconciling this simple model with detailed dust disk physics awaits even more detailed and comprehensive future observational constraints (e.g., via interferometric imaging of the disk; Kloppenborg et al. 2010).

In its simplest form, our single-temperature blackbody model for the disk is parameterized by a single scaling factor which (in conjunction with the distance to ϵ Aur) is related to the projected emitting area of the disk (hence, its size). Used in this fashion, this would correspond to a completely opaque disk that emits only from its visible projected surface area. However, as discussed in Section 3.3, we have reason to assume that the dusty disk in ϵ Aur must be partially transmissive. As discussed in Section 3.6, the completely opaque case provides only a useful limiting case for the estimation of physical parameters of the disk. This has led us to express the blackbody component scaling factor as the product of two parameters. The first of these relates to the projected surface area of the disk and the second is a disk "emissivity" factor. The latter parameter scales the blackbody flux to account for the emission of dust grains inside the partially transmissive disk that are visible from outside the disk and/or the fact that, while a true circumstellar disk likely contains a range of dust temperatures, we are utilizing only a single-temperature model. This parameter goes hand in hand with the transmissivity factor that we also assigned to the disk (see Section 3.3), which specifies how much of the flux of an object behind or inside the disk will still be visible through the disk.

Both the transmissivity and emissivity factors are physically meaningful, but purely parametric in their application to our model. The former is constrained somewhat by the value required to match the far-UV SED with a model B star spectrum. The value of the latter, however, is determined almost solely by minimizing the χ^2 of the IR ($\lambda > 1$ μm) region of the model. The caveat to this is that, in general, the emissivity would be 1.0 for a completely opaque disk in which the flux contribution from the disk is determined solely by the projected surface area—hence, dimensions and inclination—of the disk. For a more transmissive disk, the value of the emissivity factor will be larger than 1.0.

3.5. Stellar Component Masses

If the F star in ϵ Aur is a bona fide F0 supergiant (luminosity class I), then it must have a mass of $M_{\rm F} \approx 15\,M_\odot$ or more (Cox 2000). The well-known mass function of ϵ Aur, $f = 3.12\,M_\odot$ (e.g., Lissauer et al. 1996 and references therein), then requires that the mass of the B star component be $13.7\,M_\odot$ or more. This, in turn, would require the B star to be of spectral type B1 V or earlier, which is excluded by the observed far-UV SED, which constrains the spectral type to B5 $\pm$ 1 V (with a mass of $5.9 \pm 0.8\,M_\odot$; Cox 2000). Among other arguments (e.g., see Lambert & Sawyer 1986), a massive evolved B star can be excluded as a plausible scenario by considering the small relative contribution of the B star to the SED. Compared to the factor of $\gtrsim$10 increase in stellar radius between B5 and B8 stars of luminosity classes V and I (Cox 2000), such a star would be quite overluminous compared to the observed SED. Although some additional mass in the B star component can be attributed to the dust disk, it seems unlikely that $\gtrsim 8\,M_\odot$ could be accounted for in this manner (see Section 3.6 for confirmation of this).

If the B star is a B5 $\pm$ 1 V star, and assuming for the moment that the mass of the dust disk is negligible in comparison (i.e., $\ll 1\,M_\odot$), then the known mass function requires that the mass of the F star is $2.2^{+0.9}_{-0.8}\,M_\odot$. This conclusively points to the identification of the F star in ϵ Aur as a low-mass post-AGB star rather than a normal high-mass supergiant. Eggleton & Pringle (1985), Saito et al. (1987), Takeuti (1986), and Lambert & Sawyer (1986) have also suggested low-mass F star models for ϵ Aur, although only the last of these has explicitly explored a post-AGB identification; also see the review in Guinan & Dewarf (2002). Additional support for this conclusion is provided in Section 4.

3.6. Disk Size and Mass

There is considerable evidence that both the disk and the orbital plane of ϵ Aur must be viewed close to edge-on. For example, the flatness of the eclipse profile requires that if the eclipsing body is an approximately circular disk, then it must be seen in projection at a high inclination (i.e., close to edge-on). A circular disk viewed in projection at a low inclination (i.e., close to face-on) would produce a significant variation in the geometrically obscured area of the F star as the eclipse

progresses. In fact, this effect rather strongly constrains the inclination to be in the range $i \gtrsim 87^\circ$ (also see Lissauer et al. 1996).

In the limiting case where the inclination is $i = 90^\circ$, the obscuration of the F star during eclipse must be produced solely by the disk rim. We parameterize this with a disk thickness, expressed as the height measured from the disk mid-plane, $H_{\rm disk}$ (i.e., one-half of the actual geometric thickness of the disk). During eclipse, the optical–near-IR flux density is reduced by ≈50%. To first approximation, this would result if the disk completely obscured 50% of the projected area of the F star, which could be accomplished with a uniform disk having a thickness of 0.5 AU (i.e., $H_{\rm disk} = 0.25$ AU). However, in order to reproduce the observed mid-IR SED, under the assumption that the disk is completely opaque, would require a disk radius of ≈20 AU.

If the masses of the stellar components in ϵ Aur are $M_{\rm F} \approx 2.2$ and $M_{\rm B} \approx 5.9$, then we can calculate the orbital separation of the stellar components to be $a \approx 18.1$ AU, which clearly rules out a disk with a radius of 20 AU. This orbital separation, in turn, allows us to estimate the outer radius of the disk (e.g., using Equation (2) from Lissauer et al. 1996), to be $R_{\rm disk} \approx 3.8$ AU. Incidentally, the Keplerian orbital velocity at the edge of such a disk would be 37 km s^{-1} (starting from the general form of Kepler's Third Law, $r^3 = P^2 M_*$ and rearranging to yield $v_{\rm rot} = 2\pi\sqrt{M_*/r}$ for units of distance in AU, time in yr, and mass in $M_\odot$). This is comparable to the range of ≈30–40 km s^{-1} inferred for the ϵ Aur disk via observations of radial velocities of H and metal lines (e.g., Ferluga & Mangiacapra 1991; Saito et al. 1987; Lambert & Sawyer 1986).

A disk with thickness of 0.95 AU (i.e., $H_{\rm disk} = 0.475$ AU) and radius of 3.8 AU, viewed at an inclination of 89°, is sufficient to produce a geometric obscuration of the F star's disk of 72% (i.e., 28% of the F star is completely unobscured by the disk during eclipse). A disk transmissivity of 0.3 (see Section 3.3) allows 30% of the flux from the obscured portion of the F star (i.e., 22% of the total flux) to be visible through the disk, resulting in the 50% value constrained by the eclipse depth. Finally, an emissivity factor of 2.43 is required to produce the model shown in Figure 1 (i.e., the observed flux of the slightly transparent disk is a factor of 2.43 larger than would be observed if only the opaque outer surface of the disk contributed). Additional solutions at other inclinations (always $\gtrsim$87°) are possible for other combinations of disk height, transmissivity, and emissivity (e.g., Figure 1 shows the model produced by the disk parameters listed in Table 2; however, with $r_{\rm disk}$ fixed at 3.8 AU and transmissivity fixed at 0.3, identical eclipsed fraction and model SED are achieved using $i = 88^\circ$, $H_{\rm disk} = 0.725$ AU, and emissivity of 1.54, or using $i = 90^\circ$, $H_{\rm disk} = 0.375$, and emissivity of 3.41). As noted in Huang (1973, 1974), the uniqueness of disk models for ϵ Aur is problematic.

Up to this point, we have assumed that the mass of the dust disk is negligible compared to the stars in ϵ Aur. Let us now test the validity of that assumption, starting with comparisons to other astrophysical disks. For example, the dust disks around young (T Tauri) stars are found to have a sharply peaked distribution of total (gas+dust) mass centered on 0.01 $M_\odot$, with the majority of objects in the range 0.001–0.1 $M_\odot$ (Hartmann 1998). However, these disks also have characteristic sizes (outer radii) of 50–100 AU or more, implying that the ϵ Aur disk, if similar in structure, would likely be more than 2 orders of magnitude less massive (much less if we consider only the mass of dust).

Morales et al. (2009) used *Spitzer* observations of 52 A and late-B type main-sequence stars to estimate minimum dust disk masses of up to 0.6 $M_{\rm moon}$ (≈2×10^{-8} $M_\odot$). The minimum disk masses for most of their sample were several orders of magnitude smaller. They note that the total disk masses (i.e., including larger items that evade detection), assuming parent body planetesimal sizes of 1 km, could be a factor of 10^4 larger (i.e., ∼10^{-4} $M_\odot$). They modeled these disks as annular rings around the parent star, and found a median radius of 11.9 AU (range of 5–93 AU) with a radial spread of ∼3–40 AU. This would present a surface area larger by a factor of at least ∼5 than the disk in ϵ Aur, so we would expect the disk masses from Morales et al. (2009) to overestimate the ϵ Aur disk mass, if they are otherwise comparable in structure.

Another estimate of the ϵ Aur disk mass can be made by comparison to the circumbinary dust disk that produces the mid-IR excess in the cataclysmic variable V592 Cassiopeiae. This disk, which is itself the most massive dust disk yet known for a cataclysmic variable, has been modeled to contain 2.3×10^{21} g (≈10^{-12} $M_\odot$) of dust (Hoard et al. 2009). If we scale up the V592 Cas dust disk to the same volume as the ϵ Aur disk, then the mass of dust in the latter would be ∼6×10^{-5} $M_\odot$. It is not clear if this scaling up exercise is appropriate, since the morphology and, hence, presumed mass distribution of the circumbinary disk in V592 Cas is quite different (geometrically very thin compared to its radius, à la the rings of Saturn) compared to the ϵ Aur disk (which is quite thick relative to its radius, almost toroidal). However, the binary star hosts of these disks are similar in all but scale, so we might expect a scaled comparison of their dust disks to still provide some useful limiting values.

From opacity arguments, Hinkle & Simon (1987) and Backman et al. (1984) estimated disk masses of ∼10^{-6} $M_\odot$ (gas only) and ∼10^{-7} $M_\odot$ (gas and dust), respectively. We can attempt to further quantify an upper limit to the disk mass in ϵ Aur in a similar fashion. We start by assuming that the dust in the disk is comprised solely of spherical silicate grains with density of 3.0 g cm^{-3} and radius of 10 μm. If we imagine looking through a 1 cm^2 column of such grains, then on average $[(1\,{\rm cm})/(0.001\sqrt{2}\,{\rm cm\,grain^{-1}})]^2 = 5 \times 10^5$ dust grains per cm^2 would be required to produce complete geometric obscuration along the length of the column (i.e., any photon traveling along the column will inevitably be intercepted by a dust grain). The factor of $\sqrt{2}$ provides for the round cross sections of the spherical dust grains to overlap in order to completely fill a 1 cm^2 square column cross section. If the column length is of the order of the disk radius, then the mean dust grain number density is 8.8×10^{-9} cm^{-3}, corresponding to a total mass of dust in the disk of ≈8×10^{-9} $M_\odot$. Of course, there could be *more* mass than this—we cannot discriminate past the point at which the disk would be completely opaque due to the column density of dust grains. However, the fact that we do see the B star inside the disk implies that (as already assumed in our model), the disk is not completely opaque, so this mass estimate is necessarily an upper limit.

The mass of a spherical dust grain with a fixed density increases in proportion to $r_{\rm dust}^3$, while the cross section of the grain increases as $r_{\rm dust}^2$. Thus, increasing the grain radius by a factor of 10 decreases both the requisite column density to achieve total obscuration and the total number of dust grains in the disk by a factor of 10^2, but increases the total mass of the grains only by a factor of 10. In this manner, we can estimate that if the total mass of dust in the disk is ∼1 $M_\odot$ (and the disk is

completely opaque), then the "dust grains" would have to have implausibly large radii, $r_{\rm dust} \sim 1$ km.

Therefore, based on all of the comparisons and calculations described above, it appears safe to say that the mass of the dust disk in ϵ Aur is $\ll 1\,M_{\odot}$, with the range of estimates topping out at around one-hundredth of a percent of a solar mass. Presumably there is also gas in the disk, but even at the "standard" ISM gas-to-dust mass ratio of ~100:1 (Tielens 2005), the mass contribution from the gas will still leave the estimated total disk mass at well under $1\,M_{\odot}$. Plausibly large dust grains (e.g., centimeter-scale "pebbles") are expected to have distinct submillimeter emissivity properties (perhaps related to the 9 mJy 250-GHz flux density found by Altenhoff et al. 1994), and deserve further study at long wavelengths.

4. EVOLUTIONARY MODELS FOR ϵ AUR

Just after the last eclipse event of ϵ Aur, Webbink (1985) presented a few model scenarios for the evolution of the binary. Given the poorly known distance at the time and its MK spectral classification, ϵ Aur was considered an F supergiant based on its spectral characteristics (e.g., narrow lines) and effective temperature. Castelli (1978) performed a spectroscopic fine analysis to derive $\log g = 1$, indicative of a low surface gravity consistent with a very large star. Webbink (1985) assumed three possible absolute luminosities for the supergiant, bracketing the full range of the distance estimate at the time. His models for ϵ Aur initially included a pre-main-sequence star, making the binary extremely young, but then he quickly argues against such a scenario on a number of grounds. Next, Webbink (1985) considered a number of shell and core burning scenarios, all more or less suggestive that ϵ Aur was a post-main-sequence star located in one or another "loop" of its evolution crossing the Hertzsprung–Russell (H–R) diagram. Some of these loops involve significant mass loss from the star during an earlier stage.

While the general idea of the presence of a post-main-sequence evolved F star in ϵ Aur is not a new idea (e.g., see Lambert & Sawyer 1986), we have proposed here that the apparent F supergiant star is, in fact, a bright post-asymptotic giant branch (post-AGB) star that started on the main sequence as a $\gtrsim 7\,M_{\odot}$ star. The observed $^{12}C/^{13}C$ ratio of ~10 from CO line observations (Hinkle & Simon 1987) and possibly elevated barium abundance of 2× solar (Castelli 1978) are indicative of AGB thermal dredge-up and *s*-process enhancement appropriate for a post-AGB star. We note that the elevated barium abundance result from Castelli (1978) would benefit from an analysis of new observations that utilizes updated oscillator strengths and compares the barium spectral features to the line strengths of other *s*-process elements. We believe that the mass of the F star is currently near $2.2\,M_{\odot}$, while its size is that of a supergiant ($135\,R_{\odot}$). The constraints on the mass and radius of the F star, which include comparison with multi-wavelength (i.e., the SED presented here) and interferometric (e.g., Stencel et al. 2008) observations and the *HIPPARCOS* parallax distance, as well as known kinematic properties of ϵ Aur, are discussed in detail above. We justify the plausibility of the proposed low-mass, post-AGB F star below.

The study of post-AGB stars is a developing field in stellar evolution research, as more examples are identified observationally (see Szczerba et al. 2007). Among the few single star evolutionary models that come close to the post-AGB phase are those presented by Marigo & Girardi (2007), which include thermal pulse tracks for stars up to $5\,M_{\odot}$ and a range of metallicity. The inherent instabilities limit the full exploration of these extreme late phases of evolution, but such work provides guidance for interpreting the F star in ϵ Aur. Given the observational constraints on the F star, namely $T_{\rm eff}$, $R/R_{\odot}$, $\log L = 4.7$, $Z \sim Z_{\odot}$ and the ~100 d quasi-period of photospheric variations, the $5\,M_{\odot}$ tracks in Marigo & Girardi (2007) come closest to approaching these values and have evolutionary timescales approaching 10^5 yr. By extension, we could place the progenitor of the F star in the $6–8\,M_{\odot}$ range, making it a candidate for so-called super-AGB status (Smartt et al. 2009). Tidal interaction between components in ϵ Aur might account for the inflated size of the F star and some of the out-of-eclipse light variations.

The effective temperature and luminosity of the F star component in ϵ Aur matches well with an initially $7\,M_{\odot}$, post-AGB star early in its evolution away from the AGB, probably after being "born-again" by a thermal pulse due to rapid core burning. However, the evolution tracks in the H–R diagram for the initial movement away from the AGB and following a thermal pulse are indistinguishable, so we can not tell where in its post-AGB evolution the F star is actually located. In any case, these "loops" on the H–R diagram are extremely rapid for such a star, with durations of only a few thousand years (Bloecker 1995). Ancient star catalogs, however, do not imply much change in the appearance of ϵ Aur on the timescale of recorded human history (Carroll et al. 1991; Guinan & Dewarf 2002).

The known mass function of ϵ Aur requires that the F star currently has a mass of ~1–3 $M_{\odot}$ for a ~5–7 $M_{\odot}$ B star (where the range in B star mass represents the constrained range of its spectral type, B5 ± 1 V). By implication, during the past few 100,000 years, the F star must have lost ~5 or more solar masses of material during its AGB and post-AGB evolution. This high mass loss amount argues for the star being in its first or even second thermal pulse loop tour of the upper H–R diagram. The F star was the initially more massive star in the ϵ Aur binary system, starting on the main sequence as an early B star. This assignment gives ϵ Aur an age of approximately 60–80 million years since the zero-age main sequence (ZAMS).

The additional complication of binary star evolution requires further work (see Eldridge et al. 2008), but assessing the F star to be in a transitional state (blue loop) in its evolution makes an attractive and testable hypothesis. The implied 10^4 yr or longer timescales could provide ample time to transfer and lose mass in and around the binary, but not allow the resultant disk to dissipate, nor the photosphere to chemically modify due to hot bottom burning. The B5 V star and its surrounding dust disk are likely capture sites for some of the mass lost by the present-day F star, but not as much as one might think. As the precursor F star expanded after its main-sequence life was over, the binary nature of the system would have allowed matter to flow through not only the inner Lagrange point (L1, located between the two stars) but also a greater flow would have escaped through the outer Lagrange point (L2), as modeled and discussed in Eggleton & Kiseleva-Eggleton (2002) in relation to Algol-like binaries. The issue of large amounts of mass loss in close binaries, especially the idea of non-conservative mass loss through the outer Lagrange points, is famously known as the Algol Paradox and was treated in detail in Kopal (1978).

If the mass lost from ϵ Aur leaked out of the L2 side of the binary, then it might remain "hidden" in a thin, flat ring of measurable extent. Observers might look for evidence of faint, tell-tale circumbinary emission from such residual material around ϵ Aur. Taking the advanced post-AGB evolution nature of the primary star, we believe that the "supergiant" size is

due to continual mass loss via a slow expanding photosphere heading toward shell ejection as in a planetary nebula or similar type of object (e.g., Sakurai's object or FG Sagittae; Lawlor & MacDonald 2003). The inferred F star radius of 135 $R_\odot$ is consistent with these stars and the models produced for them.

5. CONCLUSIONS

We have analyzed an unprecedented SED of ϵ Aur, assembled from observational data spanning 3 orders of magnitude in wavelength. In conjunction with constraints provided by other published information about this enigmatic binary star, such as its orbital dynamics, we can conclude that (1) the F star component is a low-mass post-AGB object, (2) the B star component is a B5±1 V star, and (3) the dusty disk is a partially transparent, low-mass disk of predominantly 10 μm or larger grains. The identification of the F star in ϵ Aur as a normal high-mass F supergiant is simply no longer tenable as a plausible scenario. The requisite mass of the B star plus disk cannot be made to satisfy the well-known mass function for this system (without invoking exotic scenarios involving compact, non-luminous sources of 5–10 $M_\odot$ of additional mass that do not produce X-rays—see Section 1), while at the same time satisfying the constraints on the luminosity and SED by the data we have assembled here. From an evolutionary standpoint, the F star must have been initially the more massive of the stellar components in the binary, and some or all of the mass in the dusty disk around the B star may have been transferred from the F star precursor. The bulk of the mass is likely to have escaped from the binary during the evolution of the F star precursor, and might be visible in sensitive observations at far-IR wavelengths. As a post-AGB object, the F star is in a relatively rapid transitional phase of stellar evolution, and we should expect significant changes in the appearance of ϵ Aur after the next few thousand to tens of thousands of years. In the meantime, observational studies of the out-of-eclipse disk at wavelengths greater than 30 μm and via interferometric imaging are to be encouraged.

We thank Sally Seebode for her valuable assistance in assembling the data used in this work, and the anonymous referee, whose comments and suggestions improved the manuscript. D.W.H. thanks S. Carey and J. Surace of the IRAC Instrument Support Team for helpful discussions about the properties of the IRAC detector hardware. We give a special thanks to P. Kohler (Kohler 1992) for devising an appropriate epithet for ϵ Aur ("*le monstre invisible*"), which we have borrowed for the title of our paper. We acknowledge with thanks the variable star observations from the AAVSO International Database contributed by observers worldwide and used in this research. This work is based in part on observations made with the *Spitzer Space Telescope*, which is operated by the Jet Propulsion Laboratory, California Institute of Technology, under a contract with the National Aeronautics and Space Administration (NASA). Support for this work was provided by NASA. Some of this work was also supported by NASA through contract agreement 1275955 with the University of Denver, issued by the Jet Propulsion Laboratory, California Institute of Technology. R.E.S. is grateful to the estate of William Herschel Womble for support of astronomy at the University of Denver. This work makes use of data products from the Two Micron All Sky Survey, which is a joint project of the University of Massachusetts and the Infrared Processing and Analysis Center/Caltech, funded by NASA and the NSF. Some of the data presented in this paper were obtained from the Multimission Archive at the Space Telescope Science Institute (MAST). STScI is operated by the Association of Universities for Research in Astronomy, Inc., under NASA contract NAS5-26555. Support for MAST for non-*HST* data is provided by the NASA Office of Space Science via grant NAG5-7584 and by other grants and contracts. This research has made use of the SIMBAD database, operated at CDS, Strasbourg, France, and NASA's Astrophysics Data System.

Facilities: FUSE, HST(GHRS), IUE, AAVSO, IRAS, Spitzer(IRAC, IRS, MIPS)

REFERENCES

Ake, T. 1985, in NASA Conf. Publ. 2384, North American Workshop on the Recent Eclipse of Epsilon Aurigae, ed. R. E. Stencel (Washington, DC: NASA), 37
Ake, T. B. 2006, in ASP Conf. Ser. 348, Astrophysics in the Far Ultraviolet: Five Years of Discovery with FUSE, ed. G. Sonneborn, H. Moos, & B-G Andersson (San Francisco, CA: ASP), 156
Altenhoff, W. J., Thum, C., & Wendker, H. J. 1994, A&A, 281, 161
Altner, B. M., Chapman, R. D., Kondo, Y., & Stencel, R. E. 1984, in NASA Conf. Publ. 2349, Future of Ultraviolet Astronomy Based on Six Years of IUE Research, ed. J. M. Mead, R. D. Chapman, & Y. Kondo (Washington, DC: NASA), 365
Backman, D. E., Becklin, E. E., Cruikshank, D. P., Joyce, R. R., Simon, T., & Tokunaga, A. 1984, ApJ, 284, 799
Backman, D. E., & Gillett, F. C. 1985, ApJ, 299, L99
Barsony, M., Mould, J. R., & Lutz, B. L. 1986, PASP, 98, 637
Beckwith, S., Evans, N. J., II, Becklin, E. E., & Neugebauer, G. 1976, ApJ, 208, 390
Bessell, M. S. 1979, PASP, 91, 589
Bessell, M. S., & Brett, J. M. 1988, PASP, 100, 1134
Bloecker, T. 1995, A&A, 299, 755
Cameron, A. G. W. 1971, Nature, 229, 178
Campins, H., Rieke, G. H., & Lebofsky, M. J. 1985, AJ, 90, 896
Carroll, S. M., Guinan, E. F., McCook, G. P., & Donahue, R. A. 1991, ApJ, 367, 278
Castelli, F. 1978, A&A, 69, 23
Castelli, F., & Kurucz, R. L. 2003, in IAU Symp. 210, Modelling of Stellar Atmospheres, ed. N. Piskunov, W. W. Weiss, & D. F. Gray (San Francisco, CA: ASP), poster A20 (CD-Rom)
Chapman, R. D., Kondo, Y., & Stencel, R. E. 1983, ApJ, 269, L17
Cohen, M., Wheaton, W. A., & Megeath, S. T. 2003, AJ, 126, 1090
Cox, A. N. 2000, in Allen's Astrophysical Quantities (4th ed.; New York: Springer)
D'Alessio, P., Calvet, N., Hartmann, L., Franco-Hernández, R., & Servín, H. 2006, ApJ, 638, 314
Deming, D. 2009, IAU Symp. 253, Transiting Planets, ed. F. Pont, D. Sasselov, & M. Holman (Cambridge: Cambridge Univ. Press), 197
Egan, M. P., et al. 2003, VizieR Online Data Catalog, 5114, 0
Eggleton, P. P., & Kiseleva-Eggleton, L. 2002, ApJ, 575, 461
Eggleton, P. P., & Pringle, J. E. 1985, ApJ, 288, 275
Eldridge, J. J., Izzard, R. G., & Tout, C. A. 2008, MNRAS, 384, 1109
Fazio, G. G., et al. 2004, ApJS, 154, 10
Ferluga, S., & Hack, M. 1985, A&A, 144, 395
Ferluga, S., & Mangiacapra, D. 1991, A&A, 243, 230
Fitzpatrick, E. L., & Massa, D. 2007, ApJ, 663, 320
Guinan, E. F., & Dewarf, L. E. 2002, in ASP Conf. Ser. 279, Exotic Stars as Challenges to Evolution, ed. C. A. Tout & W. Van Hamme (San Francisco, CA: ASP), 121
Hack, M. 1959, ApJ, 129, 291
Hack, M. 1961, Mem. Soc. Astron. Ital., 32, 351
Hack, M., & Selvelli, P. L. 1979, A&A, 75, 316
Hartmann, L. 1998, Accretion Processes in Star Formation (New York: Cambridge Univ. Press), ch. 6.3
Hempel, M., & Schmitt, J. H. M. M. 2003, A&A, 408, 971
Hinkle, K. H., & Simon, T. 1987, ApJ, 315, 296
Hoard, D. W., et al. 2009, ApJ, 693, 236
Hobbs, L. M. 1969, ApJ, 157, 135
Holweger, H., Hempel, M., & Kamp, I. 1999, A&A, 350, 603
Hora, J. L., et al. 2008, PASP, 120, 1233
Houck, J. R., et al. 2004, ApJS, 154, 18
Howell, S. B., Hoard, D. W., Brinkworth, C., Kafka, S., Walentosky, M. J., Walter, F. M., & Rector, T. A. 2008, ApJ, 685, 418

Huang, S.-S. 1965, ApJ, 141, 976
Huang, S.-S. 1973, Ap&SS, 21, 263
Huang, S.-S. 1974, ApJ, 189, 485
Kloppenborg, B., et al. 2010, Nature, 464, 870
Kohler, P. 1992, Ciel Espace, 267, 34
Kopal, Z. 1971, Ap&SS, 10, 332
Kopal, Z. 1978, Astrophysics and Space Science Library (Dordrecht: Reidel), 68 (ch. 8)
Lambert, D. L., & Sawyer, S. R. 1986, PASP, 98, 389
Lawlor, T. M., & MacDonald, J. 2003, ApJ, 583, 913
Lissauer, J. J., & Backman, D. E. 1984, ApJ, 286, L39
Lissauer, J. J., Wolk, S. J., Griffith, C. A., & Backman, D. E. 1996, ApJ, 465, 371
Marigo, P., & Girardi, L. 2007, A&A, 469, 239
Mendoza, V. E. E. 1963, Bol. Obs. Tonantzintla Tacubaya, 3, 137
Morales, F. Y., et al. 2009, ApJ, 699, 1067
Mozurkewich, D., et al. 2003, AJ, 126, 2502
Natta, A., Testi, L., Calvet, N., Henning, T., Waters, R., & Wilner, D. 2007, in Protostars and Planets V, ed. B. Reipurth, D. Jewitt, & K. Keil (Tucson, AZ: Univ. Arizona Press), 767
Nordgren, T. E., Sudol, J. J., & Mozurkewich, D. 2001, AJ, 122, 2707
Parthasarathy, M., & Frueh, M. L. 1986, Ap&SS, 123, 31
Perryman, M. A. C., et al. 1997, A&A, 323, L49
Rieke, G. H., et al. 2004, ApJS, 154, 25
Saito, M., Kawabata, S., Saijo, K., & Sato, H. 1987, PASJ, 39, 135
Schmidtke, P. C., Hopkins, J. L., Ingvarsson, S. I., & Stencel, R. E. 1985, IBVS, 2748, 1
Sheffer, Y., & Lambert, D. L. 1999, PASP, 111, 829
Skrutskie, M. F., et al. 2006, AJ, 131, 1163
Smartt, S. J., Eldridge, J. J., Crockett, R. M., & Maund, J. R. 2009, MNRAS, 395, 1409
Stencel, R. 2007, in Proc. IAU Symp. 240, Binary Stars as Critical Tools and Tests in Contemporary Astrophysics, ed. W. I. Hartkopf, E. F. Guinan, & P. Harmanec (Cambridge: Cambridge Univ. Press), 202
Stencel, R. E., Creech-Eakman, M., Hart, A., Hopkins, J. L., Kloppenborg, B. K., & Mais, D. E. 2008, ApJ, 689, L137
Stickland, D. J. 1985, Obs., 105, 90
Szczerba, R., Siodmiak, N., Stasinska, G., & Borkowski, J. 2007, A&A, 469, 799
Takeuti, M. 1986, Ap&SS, 120, 1
Taranova, O. G., & Shenavrin, V. I. 2001, Astron. Lett., 27, 338
Thompson, D. T., Lutz, B. L., Lockwood, G. W., & Sowell, J. R. 1987, ApJ, 321, 450
Tielens, A. G. G. M. (ed.) 2005, in The Physics and Chemistry of the Interstellar Medium (Cambridge, UK: Cambridge Univ. Press), 153
Torres-Dodgen, A. V., & Weaver, W. B. 1993, PASP, 105, 693
Van Hamme, W. 1993, AJ, 106, 2096
Webbink, R. F. 1985, in NASA Conf. Publ. 2384, North American Workshop on the Recent Eclipse of Epsilon Aurigae, ed. R. E. Stencel (Washington, DC: NASA), 49
Werner, M. W., et al. 2004, ApJS, 154, 1
Wilson, R. E. 1971, ApJ, 170, 529
Wolk, S., Pillitteri, I., Guinan, E., & Stencel, R. 2010, AJ, submitted
Wood, K., Bjorkman, K. S., & Bjorkman, J. E. 1997, ApJ, 477, 926
Woolf, N. J. 1973, ApJ, 185, 229